Vibronic spectroscopy of Pr^{3+} in host lattices with the scheelite structure

1994 J. Phys.: Condens. Matter 6 6043

(http://iopscience.iop.org/0953-8984/6/30/022)

J. Phys.: Condens. Matter 6 (1994) 6043–6056. Printed in the UK

Vibronic spectroscopy of Pr^{3+} in host lattices with the scheelite structure

C de Mello Donegá, S Schenker†, H F Folkerts, A Meijerink and G Blasse
Debye Institute, Utrecht University, PO Box 80000, 3508 TA Utrecht, The Netherlands

Received 11 April 1994

Abstract. The luminescence spectra of Pr^{3+} in $Na_5La(MO_4)_4$ (M=Mo, W) at 4.2 K have been investigated. One- and two-phonon vibronic replicas are observed in the excitation spectra, suggesting that the contribution of the Δ process (Franck–Condon replicas) to the vibronic coupling strength of Pr^{3+} is significant. The transition probability A_{vib} for the vibronic lines in the $^3H_4 \rightarrow {}^3P_0$ excitation spectra of Pr^{3+} in several isostructural (scheelite-like) host lattices scales with the transition probability for the zero-phonon line. This is consistent with a vibronic coupling in which the Δ process dominates. The transition probabilities A_{vib} for the $^3H_4 \rightarrow {}^3P_2$ excitation and the $^3P_0 \rightarrow {}^3F_2$ emission transitions, and the vibronic spectra of Pr^{3+} in $Na_5La(MO_4)_4$ give additional support for this conclusion.

1. Introduction

The intraconfigurational $4f^n$ spectra of rare-earth (RE) ions often show weak vibronic features, despite the shielding of the 4f electrons by the $5s^2$ and $5p^6$ outer shells. Two mechanisms, namely the M and the Δ processes, can contribute to the vibronic coupling strength of RE ions [1]. The M process describes vibrationally-induced electric-dipole (ED) $4f^n$–$4f^n$ transitions. Coupling with a vibrational mode leads to an admixture of opposite parity configurations in the $4f^n$ configurations [1–3]. A detailed theoretical treatment of the M process vibronics has been carried out by Judd [4] and by Faulkner and Richardson [5] for an isolated $RECl_6^{3-}$ octahedral complex, using second-order perturbation theory. These theoretical approaches predict that vibronic transitions due to the M process obey selection rules, i.e. $U^{(2)} \neq 0$ and coupling with odd-parity vibrations only [4, 5]. The Δ process vibronic transitions, also known as Franck–Condon phonon replicas, result from a difference between the equilibrium RE-ligand distances in the ground state and in the excited state, which leads to non-zero Franck–Condon vibrational overlap factors between the ground and the excited states [1–3]. In this case the $4f^n$-$4f^n$ transitions are magnetic dipole MD allowed or partially ED allowed by the odd part of the static crystal field, and the offset between the ground state and the excited state parabolae simply causes a redistribution of the total transition intensity between zero-phonon and vibronic lines [2].

For a transition within the $4f^n$ shell the Δ process is usually neglected, since the Huang–Rhys coupling factor is assumed to be zero. There is evidence, however, that this approximation is not justified (e.g. [3, 6–10]). As we have previously pointed out [7], the

† Permanent address: Institut für Anorganische Chemie, Universität Bern, Freiestraße 3, CH-3000 Bern 9, Switzerland.

0953-8984/94/306043+14$19.50

vibronic transitions of Pr^{3+} violate the M process selection rules, suggesting a contribution by the Δ process. The observation of vibronic transitions in the intraconfigurational two-photon excitation spectrum of Pr^{3+} in $SrMoO_4$ [8] gives direct proof that the Δ process contributes to the vibronic coupling strength of Pr^{3+}, since the M process contribution is expected to vanish for two-photon transitions. The latter point has been experimentally confirmed for Eu^{2+} in $LiBaF_3$ [9].

To obtain additional support for the conclusion above, we have investigated the luminescence spectra of Pr^{3+} in $Na_5La(MO_4)_4$ (M=Mo, W), aiming at identifying two-phonon vibronic transitions, which are expected for the Δ process only [1]. These host lattices are particularly suited for our purposes, since their vibrational spectra show a distinct 400 cm^{-1} energy gap between the bending and the stretching vibrations of the MO_4^{2-} group, in addition to a clear cut-off at about 900 cm^{-1} [11]. These characteristics make it possible to observe well-defined two-phonon replicas.

In addition, a comparison between the transition probabilities A_{vib} of vibronic transitions in the $^3H_4 \rightarrow {}^3P_0$ excitation spectra of Pr^{3+} in several isostructural (scheelite-like) host lattices, namely $LiYF_4$, $LaNbO_4$, $Na_5La(WO_4)_4$, and, $Na_5La(MoO_4)_4$, will be presented.

2. Experimental details

Powder samples of composition $Na_5La_{1-x}Pr_x(MO_4)_4$ (M=Mo, W; $x = 5 \times 10^{-4}$ and 5×10^{-3}) were obtained by firing a stoichiometric mixture of Na_2CO_3, $(La_{1-x}Pr_x)_2O_3$, and MO_3 at 630 °C (M=W) or 600 °C (M=Mo) for 6 h, under air, based on the method described in [12]. The $(La_{1-x}Pr_x)_2O_3$ samples were prepared as described in [13]. The preparations of $La_{1-y}Pr_yNbO_4$ and $LiY_{1-y}Pr_yF_4$ ($y = 1 \times 10^{-3}$) have been described elsewhere ([13, 14], respectively). The samples were checked by x-ray powder diffraction and appeared to be a single phase. Absence of Pr^{4+} or other optical impurities was verified by diffuse reflectance spectroscopy.

The compounds $Na_5RE(MO_4)_4$ (RE=Rare-Earth(III); M=Mo(VI), W(VI)) crystallize in a structure which is related to the scheelite structure, with space group $I4_1/a$ [15, 16]. The RE^{3+} ions occupy the same crystallographic positions as the divalent cations in the scheelite structure, with site symmetry S_4 [15, 16]. $RENbO_4$ has the M-fergusonite structure, which is a monoclinic distortion of the scheelite structure, with space group $I2/c$ and site symmetry C_2 for the RE^{3+} ions [17]. $LiYF_4$ has the inverse scheelite structure, with space group $I4_1/a$ and site symmetry S_4 for the Y^{3+} ions [18].

The vibrational spectra of $Na_5La(MO_4)_4$ (M=Mo, W) were measured by the spectrochemical analysis group at Utrecht University. The Raman spectra were recorded between 200 and 1000 cm^{-1} with a Perkin–Elmer 1760-X FT-Raman spectrometer, irradiating the sample with a Nd:YAG laser. The infrared absorption spectra were measured between 250 and 2000 cm^{-1} using a Perkin–Elmer 2000 FT-IR spectrometer and standard pellet techniques. The low-resolution luminescence spectra were measured by using a SPEX DM3000F spectrofluorometer with 0.22 m SPEX 1680 double monochromators and a 450 W Xe Lamp, and are corrected for the instrumental response. High-resolution and decay measurements were performed on an excimer laser pumped dye laser set-up, which has been described in detail elsewhere [7].

3. Results and Discussion

3.1. Low-resolution measurements

The excitation spectra of the $^3P_0$ emission of Pr^{3+} in $Na_5La(MO_4)_4$ (M=Mo, W) consist of several lines in the region 420–490 nm, corresponding to transitions within the $4f^2$ configuration, and a broad band in the UV region. This band has a maximum at 240 nm for the tungstate and at 280 nm for the molybdate. The luminescence properties of the MO_4^{2-} groups are well known [19]. In $Na_5La(WO_4)_4$ this luminescence consists of a broad emission band with a maximum at 480 nm upon 240 nm excitation. Since excitation of $Na_5La(WO_4)_4$:0.05 mol% Pr^{3+} at 240 nm yields both Pr^{3+} and WO_4^{2-} emission, the 240 nm excitation band is ascribed to the excitation of the Pr^{3+} ions via the tungstate groups. The Pr^{3+} emission is the same as under f–f (^3P_J, $^1I_6$) excitation and will be discussed below.

Optical transitions of molybdates are known to occur at lower energies than those of the isostructural tungstates [19]. Consistently, the broad excitation band of the Pr^{3+} emission in $Na_5La(MoO_4)_4$ with a maximum at about 280 nm is ascribed to the excitation of the Pr^{3+} ions via the molybdate groups, since it yields both Pr^{3+} and molybdate emission. The latter consists of a broad band with a maximum at about 620 nm. The Pr^{3+} emission is essentially the same as under ^3P_J, $^1I_6$ excitation (see figure 2 below). The $4f^2 \rightarrow 4f5d$ transition of Pr^{3+} probably contributes to the intensity of the broad-band excitation as well, but is not clearly observed due to the low Pr^{3+} concentration.

We turn now to the intraconfigurational excitation spectra of the $^3P_0$ emission of Pr^{3+} in $Na_5La(MO_4)_4$ (M=W, Mo). Figure 1 shows the excitation spectrum of the $^3P_0 \rightarrow {}^3F_2$ emission of Pr^{3+} in $Na_5La(WO_4)_4$:0.05 mol% Pr^{3+} at 4.2 K. The intraconfigurational excitation spectrum of the $^3P_0$ emission of Pr^{3+} in $Na_5La(MoO_4)_4$ is very similar to that of Pr^{3+} in $Na_5La(WO_4)_4$, apart from a shift towards lower energies. This shift amounts to 67 cm^{-1} for the $^3H_4^{(1)} \rightarrow {}^3P_0$ zero-phonon line, and can be seen as evidence that the Pr^{3+} ions experience a larger degree of covalency in the molybdate lattice. The spectra consist of several sharp lines corresponding to transitions within the $4f^2$ configuration ($^3H_4^{(1)} \rightarrow {}^3P_{0,1,2}$ and $^1I_6$). The superscript (1) indicates the lowest crystal-field component of the $^3H_4$ ground level, which is the only one significantly populated at 4.2 K. Vibronic sidebands are clearly observed on the higher energy side of the zero-phonon lines. The integrated intensity ratio R between the vibronic features and the zero-phonon line(s) can be calculated for the $^3H_4^{(1)} \rightarrow {}^3P_0$ and $^3H_4^{(1)} \rightarrow {}^3P_2$ transitions. The analysis of the vibronic lines of the $^3H_4^{(1)} \rightarrow {}^3P_1, {}^1I_6$ transitions is complicated due to the large crystal-field splitting of the final levels (i.e. $\sim$ 1000 cm^{-1}), giving rise to several zero-phonon origins and to overlap between vibronic and zero-phonon lines.

The $^3H_4^{(1)} \rightarrow {}^3P_1, {}^1I_6$ lines start at about 500 cm^{-1} above the $^3H_4^{(1)} \rightarrow {}^3P_0$ zero-phonon line, imposing 470 cm^{-1} as an upper limit on the frequency of the vibronics included in the ratio R. The ratio R for the $^3H_4^{(1)} \rightarrow {}^3P_0$ transition is thus underestimated, since the highest vibrational frequency of $Na_5La(MO_4)_4$ is 940 cm^{-1} for M=Mo and 960 cm^{-1} for M=W, as estimated by us from the vibrational spectra. The ratio R for the $^3H_4^{(1)} \rightarrow {}^3P_2$ transition includes vibronic lines up to 1100 cm^{-1}, but lines with frequency lower than 100 cm^{-1} overlap with the tail of the electronic lines. This leads to a larger uncertainty in the R values for this transition. The estimated uncertainties are some 20% for the $^3H_4^{(1)} \rightarrow {}^3P_2$ transition and some 10% for the $^3H_4^{(1)} \rightarrow {}^3P_0$ transition. The values for the latter transition are more accurate, because only one zero-phonon line is observed, the $^3P_0$ level being non-degenerate.

The underestimation of R for the $^3H_4^{(1)} \rightarrow {}^3P_0$ transition can be corrected for by assuming

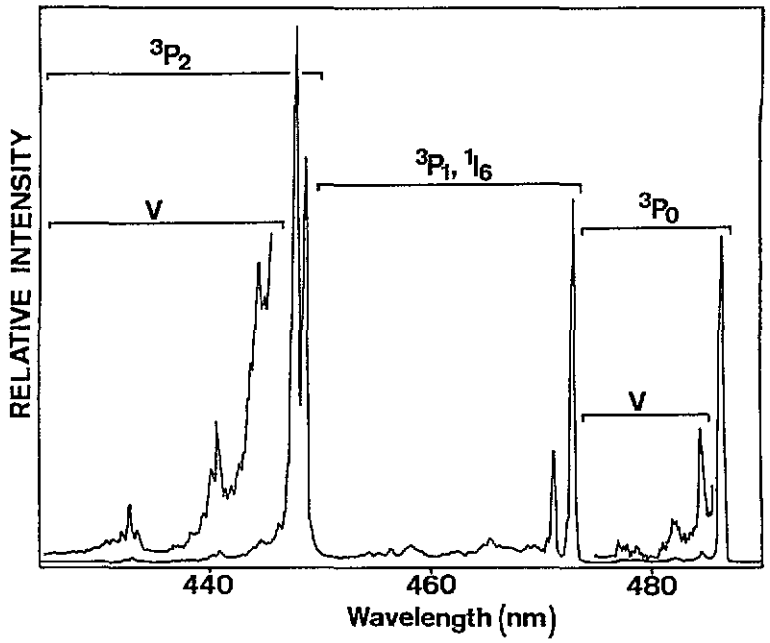

Figure 1. The intraconfigurational excitation spectrum ($^3H_4^{(1)} \rightarrow {}^3P_{0,1,2}$, $^1I_6$ transitions) of the $^3P_0 \rightarrow {}^3F_2$ emission of Pr^{3+} in $Na_5La(WO_4)_4$:0.05 mol% Pr^{3+} at 4.2 K. The final levels are indicated. The label V indicates the vibronic sidebands. The upper lines show the vibronic part of the $^3H_4^{(1)} \rightarrow {}^3P_{0,2}$ transitions magnified by a factor 10.

that the contribution of vibronic lines with frequencies higher than 470 cm^{-1} is similar for both $^3H_4^{(1)} \rightarrow {}^3P_0$ and $^3H_4^{(1)} \rightarrow {}^3P_2$ transitions. This assumption is justified, since the intensity of the vibronic lines between 260 and 470 cm^{-1} relative to the zero-phonon lines is not significantly different for the two transitions. The estimated R values for the $^3H_4^{(1)} \rightarrow {}^3P_0$ and the $^3H_4^{(1)} \rightarrow {}^3P_2$ excitation transitions are, respectively, 0.14 (0.17) and 0.23 for the molybdate, and 0.12 (0.14) and 0.21 for the tungstate. The corrected R values are given between brackets. At first glance, these R values seem to indicate that the vibronic coupling strength of Pr^{3+} is the same in both host lattices. However, for a better comparison one has to consider the transition probabilities for the vibronic transitions of Pr^{3+} in both host lattices. This will be done in section 3.3.

The emission spectra of Pr^{3+} in $Na_5La(MO_4)_4$ for M=Mo and M=W are very similar. As an example, figure 2 shows the emission spectrum of $Na_5La(MoO_4)_4$:0.05 mol% Pr^{3+} at 4.2 K, upon $^3P_2$ excitation. The emission lines correspond to the transitions $^3P_0 \rightarrow {}^3H_{4,5,6}, {}^3F_{2,3,4}$ and $^1D_2 \rightarrow {}^3H_{4,5}$ (figure 2). The emission lines in the tungstate lattice are shifted to higher energies, indicating a lower degree of covalency for the Pr–O bonds in this host lattice. The shift of the $^3P_0$ emission lines, 60 cm^{-1}, is larger than that of the $^1D_2$ lines, 25 cm^{-1}. Similar observations have been reported before for Pr^{3+} in several host lattices (e.g. [10, 20, 21]), but are not well understood. A possible explanation for this phenomenon is that the triplet 4f5d states are at lower energies than the singlet 4f5d states. A better admixture of the triplet 4f5d states into the triplet states of the $4f^2$ configuration causes those levels to shift more than the singlet levels upon lowering of the 4f5d states due to increasing covalency [22].

The most remarkable difference between the emission spectra of Pr^{3+} in the two host

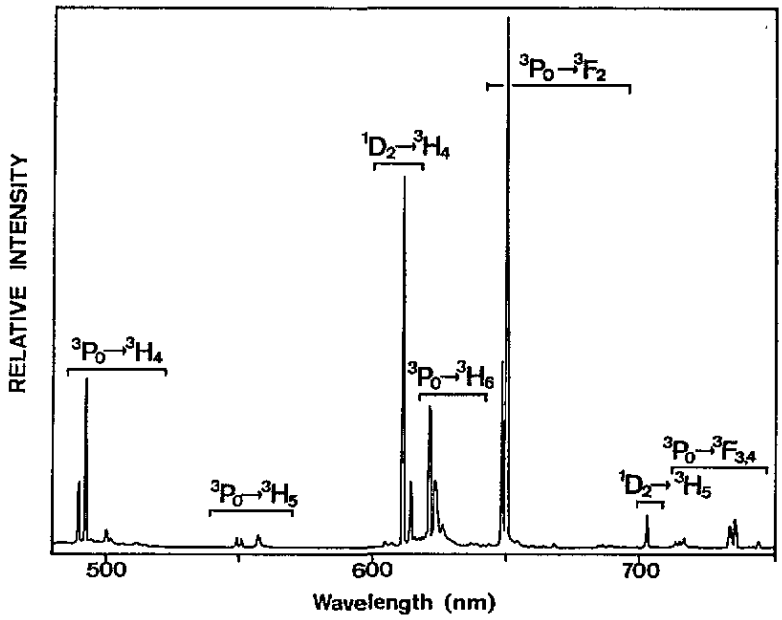

Figure 2. The emission spectrum of $Na_5La(MoO_4)_4$:0.05 mol% Pr^{3+} at 4.2 K upon $^3P_2$ excitation.

lattices is the larger relative intensity of the $^1D_2$ emission in $Na_5La(MoO_4)_4$:Pr, namely 30% compared to 15% in the isostructural tungstate. A detailed discussion of this point lies beyond the scope of this paper, and will be presented elsewhere [23], together with the analysis of the non-radiative relaxation rates of Pr^{3+} in $Na_5RE(MO_4)_4$ (RE=Y, La, Gd, Lu; M=Mo, W) and $RENbO_4$ (RE=Y, La).

Vibronic transitions are also observed in the emission spectrum. The $^3P_0 \rightarrow ^3F_2$ is the most suitable emission transition for a quantitative analysis of the intensity of the vibronic lines, because the crystal-field splitting of the $^3F_2$ level is small ($\sim$40 cm^{-1}) compared to the frequency of the vibronic transitions and only two zero-phonon lines are observed. Vibronic lines can be observed on the lower energy side of the zero-phonon lines. The vibronic spectra will be discussed below (section 3.2). The integrated intensity ratio R for the vibronics is 0.10 for Pr^{3+} in the tungstate and 0.13 for Pr^{3+} in the molybdate lattice.

3.2. High-resolution measurements

The vibronic part of the $^3H_4^{(1)} \rightarrow ^3P_0$ high-resolution excitation spectra of the $^3P_0 \rightarrow ^3F_2$ emission of Pr^{3+} in $Na_5La(MO_4)_4$ (M=Mo, W) is shown in figure 3. The vibronic part of the $^3H_4^{(1)} \rightarrow ^3P_2$ high-resolution excitation spectrum of the $^3P_0 \rightarrow ^3F_2$ emission of Pr^{3+} was measured only for Pr^{3+} in $Na_5La(WO_4)_4$, and is shown in figure 4. The $^3P_0 \rightarrow ^3F_2$ transition is the most suitable emission transition to investigate the vibronic spectra, since the crystal-field splitting of the $^3F_2$ level is small (i.e. 40 cm^{-1}) compared to the frequencies of the vibronic transitions and only two zero-phonon lines are observed, at 15 442 cm^{-1} and 15 400 cm^{-1} for Pr^{3+} in the molybdate, and 15 494 cm^{-1} and 15 456 cm^{-1} in the tungstate. The relative intensities of these lines are 3:10 in both host lattices. Vibronic lines can be observed on the lower energy side of the zero-phonon lines. Figure 5 compares the vibronic part of the $^3P_0 \rightarrow ^3F_2$ emission spectra of Pr^{3+} in $Na_5La(MO_4)_4$ for M=Mo (figure 5(*a*))

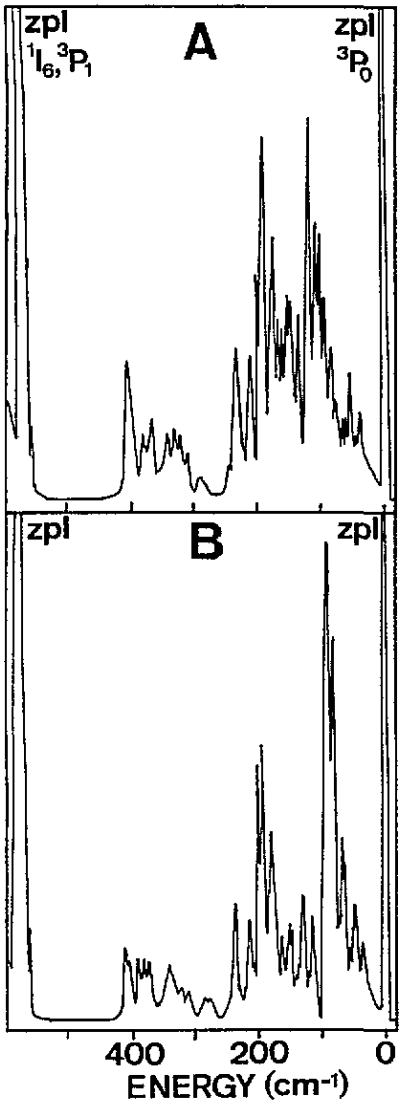

Figure 3. The vibronic part of the $^3H_4^{(1)} \rightarrow ^3P_0$ high-resolution excitation spectra of the $^3P_0 \rightarrow ^3F_2$ emission of Pr^{3+} in $Na_5La(MO_4)_4$ at 4.2 K for (**A**) M=Mo, and (**B**) M=W. The $^3H_4^{(1)} \rightarrow ^3P_0$ zero-phonon line (ZPL) is at 20463 cm^{-1} for M=Mo, and 20530 cm^{-1} for M=W. One of the $^3H_4^{(1)} \rightarrow ^3P_1$, $^1I_6$ ZPLs is also indicated. The spectra are not corrected for the variation of the dye laser output with wavelength.

and M=W (figure 5(*b*)).

Figures 3 and 5 show that the vibronic spectra of Pr^{3+} in the two host lattices are very similar, as expected considering that the host lattices are isostructural and the Pr^{3+} ions substitute for La^{3+} in both cases. The observed vibronic spectra show remarkable fine structure. The frequencies of the vibronic lines nearly coincide with those of the $k = 0$ phonons of the host lattices, except for the line at 405 (M=Mo) or 412 cm^{-1} (M=W) from the zero-phonon origin. As an example, table 1 compares the vibronic spectra of Pr^{3+} in $Na_5La(WO_4)_4$ and the vibrational data of the host lattice. The assignment of the

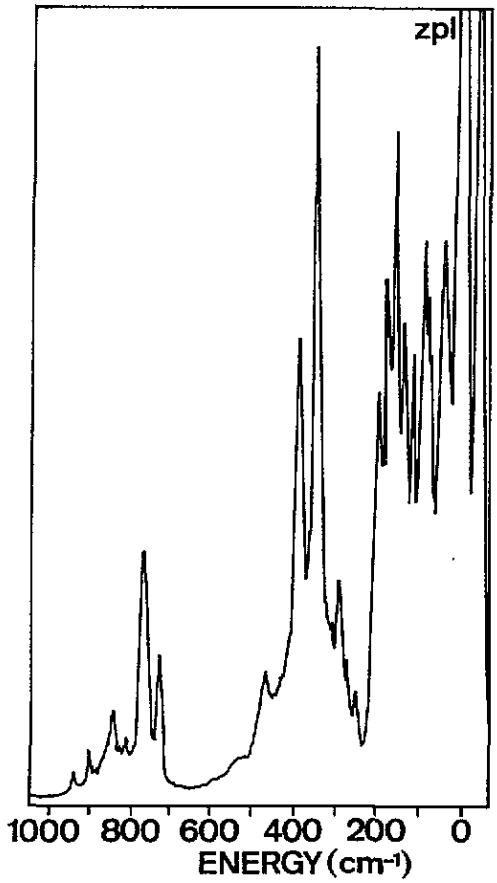

Figure 4. The vibronic part of the $^3H_4^{(1)} \rightarrow {}^3P_2$ high-resolution excitation spectrum of the $^3P_0 \rightarrow {}^3F_2$ emission of Pr^{3+} in $Na_5La(WO_4)_4$ at 4.2 K. The $^3H_4^{(1)} \rightarrow {}^3P_2$ ZPLs are at 22 287 and 22 247 cm^{-1}, the former being taken as the origin. The spectrum is not corrected for the variation of the dye laser output with wavelength.

vibrational modes is made by comparison with the vibrational data reported by Baran *et al* [11] for the isostructural $Na_5RE(MO_4)_4$ compounds (RE=Sm to Lu; M=Mo, W). The labels ν_1 and ν_3 indicate the symmetric and the antisymmetric stretching vibrations of the WO_4^{2-} group, respectively. The symmetric and antisymmetric bending vibrations of the WO_4^{2-} group are denoted by ν_2 and ν_4, respectively. The vibronic lines can be divided into two categories: those due to coupling with lattice vibrations (below 300 cm^{-1}) and those due to coupling with internal vibrations (i.e. bending and stretching) of the MO_4^{2-} groups (above 300 cm^{-1}). The latter is an example of co-operative vibronic transitions [24], since the Pr^{3+} ion is not directly involved in the vibration. The literature contains several examples of such transitions (see e.g. [3]).

It is seen in table 1 that there is a good agreement between the positions of the vibronic lines in the $^3P_0 \rightarrow {}^3F_2$ emission and in the $^3H_4 \rightarrow {}^3P_{0,2}$ excitation spectra. A comparison between figures 3–5 shows that the intensity distribution among the several vibronic lines is different for each transition, particularly for the $^3H_4 \rightarrow {}^3P_2$ excitation spectra. Analysis of table 1 and figures 3–5 indicates that the intensity of the vibronic lines is not determined

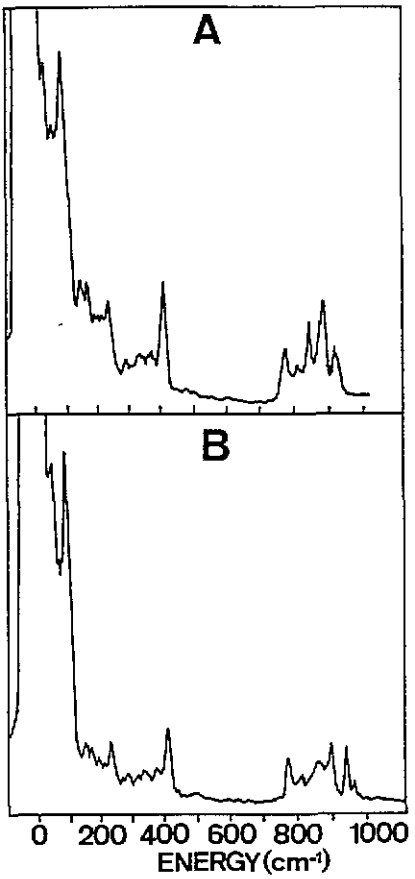

Figure 5. The vibronic part of the $^3P_0 \rightarrow {}^3F_2$ high-resolution emission spectra of Pr^{3+} in $Na_5La(MO_4)_4$ at 4.2 K upon $^3P_0$ excitation for (A) M=Mo and (B) M=W. The zero-phonon origin is at 15400 cm^{-1} for M=Mo and at 15456 cm^{-1} for M=W. The onset of the ZPLs appears on the extreme left side of the spectra.

by the Raman- or IR-active character of the phonons that couple to the electronic transition or by their oscillator strength. We note that this observation is not conclusive regarding the nature of the vibronic coupling. Despite the observed vibronic spectra being consistent with a large contribution of the Δ process, they cannot exclude the possibility of a significant contribution of the M process, since the Raman-active vibrations are not even-parity with respect to the Pr^{3+} site.

3.3. Transition probabilities

We shall now estimate the transition probabilities A_{vib} for the vibronic transitions in the $^3H_4^{(1)} \rightarrow {}^3P_0$ excitation spectra of Pr^{3+} in $LaNbO_4$ and $Na_5La(MO_4)_4$ (M=W, Mo). The value of A_{vib} can be estimated as follows

$$R = \frac{I_{vib}}{I_{zp}} = \frac{A_{vib}}{A_{zp}} \tag{1}$$

Table 1. The relative positions of the vibronic lines in the $^3H_4 \rightarrow {}^3P_{0,2}$ excitation spectra of the $^3P_0$ emission (figures 3(*b*) and 4) and in the $^3P_0 \rightarrow {}^3F_2$ emission spectrum (figure 5(*b*)) of Pr^{3+} in $Na_5La(WO_4)_4$ at 4.2 K. Vibrational data of $Na_5La(WO_4)_4$ are included for comparison. All values are in cm^{-1}. R: Raman, IR: infrared, w: weak, m: medium, s: strong, n.m.: not measured due to spectral overlap with electronic lines, —: not observed.

Vibrational frequency	Vibronic position			
	$^3H_4^{(I)} \rightarrow {}^3P_0$	$^3H_4^{(I)} \rightarrow {}^3P_2$	$^3P_0 \rightarrow {}^3F_2$†	Assignment‡
	50;70	40	50	
	80,90	90	95	
	115;130	115;135		
	150;180	155;175	155;175	Lattice
200 (R, w)	195;200	—	200	modes
235 (R, w); 253 (R, w)	235	250	240	
311 (R, w); 288 (IR, m)	280;310	290	290	
333 (R, m); 320 (IR, m)	320	—		ν_2
343 (R, m)	345	350	345	
363 (R, w); 358 (IR, w)	370	—		
381 (R, w); 385(IR, m)	377;390	385	385	ν_4
—	410	—	415	
460 (IR, w)	—	465	500	
770 (R, w); 778 (IR, s)	n.m.	730;765	775	ν_3
808 (R, w); 825 (R, w)	n.m.	820	815	
837 (R, w); 830 (IR, s)	n.m.	840	—	
875 (R, m); 850(IR, s)	n.m.	—	865	
892 (IR, m)	n.m.	900	900	
935 (R, s); 936 (IR, m)	n.m.	935	945	ν_1
956 (R, w)	n.m.	—	970	

† Relative to the most intense electronic origin.
‡ ν_i relate to the internal MO_4^{2-} vibrations.

and

$$A_{zp} = A_{^3P_0} \times \frac{I_{(^3P_0 \rightarrow {}^3H_4^{(I)})}}{I_{^3P_0}} \tag{2}$$

where $I_{^3P_0}$ and $I_{(^3P_0 \rightarrow {}^3H_4^{(I)})}$ are the integrated intensities of the total $^3P_0$ emission spectrum and of the $^3P_0 \rightarrow {}^3H_4^{(I)}$ emission line, respectively. It is assumed that the transition probabilities for the $^3H_4^{(I)} \leftrightarrow {}^3P_0$ transition are the same in absorption and emission. The radiative transition probability $A_{^3P_0}$ is estimated from the decay time τ of the $^3P_0$ level at 4.2 K, after taking account of the non-radiative decay rate. The non-radiative contribution is estimated from the relative intensity of the $^1D_2$ emission, since the $^3P_0 \rightarrow {}^1D_2$ relaxation is the only probable non-radiative decay process at low Pr^{3+} concentrations ($x \leqslant 1 \times 10^{-3}$) [25–27]. A detailed description of this method has been given before [7, 10].

The values of $I_{(^3P_0 \rightarrow {}^3H_4^{(I)})}$, $I_{^3P_0}$, and $I_{^1D_2}$ are determined after correction of the emission spectra for the instrumental response and conversion to a photon flux per energy interval scale. The ratio R is determined from the corrected excitation spectra, using the procedure described in section 3.1, and includes the complete vibronic spectra. The excitation spectrum

of the $^3P_0$ emission of Pr^{3+} in $LaNbO_4$ has been published before [13]. The concentration of Pr^{3+} ions is 0.05 mol% in $Na_5La(MO_4)_4$ (M=Mo, W) and $LaNbO_4$, and 0.1 mol% in $LiYF_4$. These concentrations are low enough to prevent reabsorption of the $^3P_0 \rightarrow {}^3H_4^{(1)}$ emission line (which leads to underestimation of A_{vib}), concentration quenching of the $^1D_2$ emission, or saturation effects in the excitation spectra [13] (which lead to overestimation of A_{vib}). The estimated A_{vib} values for the $^3H_4^{(1)} \rightarrow {}^3P_0$ excitation transition and other relevant data are summarized in table 2. The optical absorption edge is estimated from the diffuse reflectance spectra. The position of the optical absorption edge of $LiYF_4$ is assumed to be similar to that of LaF_3 [7].

Table 2. Transition probabilities for the vibronic lines and the ZPL (A_{vib} and A_{zp}, respectively) for the $^3H_4^{(1)} \rightarrow {}^3P_0$ excitation spectra of Pr^{3+} in several isostructural host lattices. The positions of the ZPL and of the optical absorption edge (OAE) of the lattice are also given. All measurements were performed at 4.2 K.

Host	R	A_{zp}	A_{vib}	τ	Spectral position (cm^{-1})	
		(s^{-1})	(s^{-1})	(μs)	ZPL	OAE
$LiYF_4$†	0.12	840	100	48	20873	80000
$LaNbO_4$	0.15	8000	1200	3.1	20534	40000
$Na_5La(WO_4)_4$	0.14	9500	1400	2.7	20530	42000
$Na_5La(MoO_4)_4$	0.17	28000	4800	0.9	20463	36000

† After [7].

Table 2 shows that A_{vib} increases by a factor 50 from $LiYF_4$ to $Na_5La(MoO_4)_4$, following the shift of the zero-phonon line and of the optical absorption edge of the host lattice to lower energies. These shifts can be ascribed to two related effects: the increase of the degree of covalency and of the polarizability of the ligands. These observations are consistent with the results previously reported by us for Pr^{3+} in several host lattices [7, 10]. We have shown before [7], that the host lattice dependence of A_{vib} can be accounted for by the influence of the polarizability of the ligands, of the degree of covalency and of the position of the opposite-parity states on the vibronic coupling strength due to the M and/or the Δ processes.

The presently observed host lattice dependence of A_{vib} is consistent with a large contribution of the Δ process to the intensity of the vibronic transitions. As can be seen in table 2, the increase of A_{vib} scales with that of A_{zp}, as is to be expected for Δ process vibronic transitions, where $A_{vib}=A_{zp} \times S \times e^{-S}$ (for one-phonon replicas) [28]. We note that the increase of A_{vib} from $LiYF_4$ to $LaNbO_4$ and from $Na_5La(WO_4)_4$ to $Na_5La(MoO_4)_4$ is larger than the respective increase of A_{zp}. This fact can be attributed to an increase of both A_{zp} and S. As we pointed out before [7], the Huang–Rhys coupling factor S is expected to increase with increasing covalency.

To show that the presently observed vibronic transitions do not obey the $U^{(2)} \neq 0$ selection rule, we estimated the values of A_{vib} and A_{zp} for the $^3H_4^{(1)} \rightarrow {}^3P_2$ excitation and the $^3P_0 \rightarrow {}^3F_2$ emission transitions of Pr^{3+} in $Na_5La(WO_4)_4$, by using the method described above. For these transitions the vibronic spectra consist of lines belonging to two intense zero-phonon origins. To estimate the transition probability A_{vib} for the vibronic lines belonging to each origin, we will assume that the ratio $R^{(\mu)}$ between the integrated intensities of the vibronic lines and the zero-phonon line is the same for transitions to different crystal-field components μ of the same level, so that $R^{(\mu)}$ is equal to the ratio R between the total integrated intensities of the vibronic lines and the two zero-phonon lines. We note that this assumption is necessary, but it introduces a larger uncertainty in the A_{vib} values, since the

vibronic coupling strength for transitions from or to different crystal-field components of the same level can be different, as shown for Eu^{2+} in $LiBaF_3$ [29].

Table 3. Transition probabilities for the vibronic and the zero-phonon lines (A_{vib} and A_{zp}, respectively) for the $^3H_4^{(1)} \rightarrow {}^3P_{0,2}$ excitation and the $^3P_0 \rightarrow {}^3F_2$ emission spectra of Pr^{3+} in $Na_5La(WO_4)_4$. The squared matrix elements $(U^{(\lambda)})^2$ (from reference [30]) for each transition are also given. All measurements were performed at 4.2 K.

Transition	R	A_{zp} (10^4 s^{-1})	A_{vib} (10^4 s^{-1})	$(U^{(2)})^2$	$(U^{(4)})^2$	$(U^{(6)})^2$
$^3H_4^{(1)} \rightarrow {}^3P_0$	0.14	0.95	0.11	0	0.1713	0
$^3H_4^{(1)} \rightarrow {}^3P_2^{(1)}$	0.21	1.38	0.27	0.00006	0.036	0.1373
$^3H_4^{(1)} \rightarrow {}^3P_2^{(2)}$	0.21	2.14	0.43	0.00006	0.036	0.1373
$^3P_0 \rightarrow {}^3F_2^{(1)}$	0.10	11	1.1	0.2943	0	0
$^3P_0 \rightarrow {}^3F_2^{(2)}$	0.10	3.3	0.33	0.2943	0	0

The values of A_{vib} for the $^3H_4^{(1)} \rightarrow {}^3P_2^{(\mu)}$ excitation and the $^3P_0 \rightarrow {}^3F_2^{(\mu)}$ emission transitions of Pr^{3+} can then be estimated by equation (1) and taking

$$A_{zp(^3P_0 \rightarrow {}^3F_2^{(\mu)})} = A_{^3P_0} \times \frac{I_{(^3P_0 \rightarrow {}^3F_2^{(\mu)})}}{I_{^3P_0}} \tag{3}$$

and

$$A_{zp(^3H_4^{(1)} \rightarrow {}^3P_2^{(\mu)})} = A_{ZP(^3H_4^{(1)} \rightarrow {}^3P_0)} \times \frac{I_{(^3H_4^{(1)} \rightarrow {}^3P_2^{(\mu)})}}{I_{(^3H_4^{(1)} \rightarrow {}^3P_0)}}. \tag{4}$$

The estimated A_{vib} and A_{zp} values are given in table 3, together with the squared matrix elements $(U^{(\lambda)})^2$ [30] for each transition. Table 3 shows that the transition probabilities A_{vib} roughly scale with the sum of the $(U^{(\lambda)})^2$ values. Furthermore, the R values for the three transitions are not significantly different. These facts imply that the $U^{(2)} \neq 0$ selection rule is not operative. If this selection rule were important, one should expect a significantly larger value for both A_{vib} and R for the $^3P_0 \rightarrow {}^3F_2^{(\mu)}$ transitions (large $U^{(2)}$) than for the $^3H_4^{(1)} \rightarrow {}^3P_0$ and $^3H_4^{(1)} \rightarrow {}^3P_2$ transitions, in clear contradiction with the results in table 3. This suggests either that the vibronic coupling strength is dominated by the Δ process contribution or that the $U^{(2)}$ selection rule for the M process is lifted. The latter possibility has been pointed out before by us [7], by analogy with the lifting of the $\Delta J \leqslant 2$ selection rule for two-photon absorption transitions when higher-order (third or fourth) perturbation terms are taken into account [31, 32].

3.4. Two-phonon replicas

As mentioned in the introduction, the recently reported observation of vibronic transitions in the two-photon $^3H_4^{(1)} \rightarrow {}^3P_0$ excitation spectra of Pr^{3+} in $SrMoO_4$ [8] gives direct evidence that the Δ process contribution to the vibronic coupling strength of Pr^{3+} is significant. We will report below new evidence supporting this conclusion, namely the observation of two-phonon vibronic replicas. The best transition to investigate the presence of two-phonon replicas is the $^3H_4^{(1)} \rightarrow {}^3P_2$ excitation, because the crystal-field splitting of the $^3P_2$ level is small (i.e. 40 cm^{-1}) compared to the frequencies of the vibronic transitions, and higher electronic levels are absent for several 10 000 cm^{-1} [33]. Figure 6 depicts part of the low-resolution $^3H_4^{(1)} \rightarrow {}^3P_2$ excitation spectrum of the $^3P_0 \rightarrow {}^3F_2$ emission of Pr^{3+} in

$Na_5La(MoO_4)_4$:0.5 mol% Pr^{3+} at 4.2 K, showing a vibronic side band located at ~800 cm^{-1} from the zero-phonon origin. Under magnification a vibronic feature can be observed at ~1600 cm^{-1} from the zero-phonon origin. Since the vibrational spectra of the host lattice show a clear cut-off at 940 cm^{-1}, these two vibronic features at 800 and 1600 cm^{-1} are ascribed to one- and two-phonon replicas due to coupling with the molybdate stretching vibration.

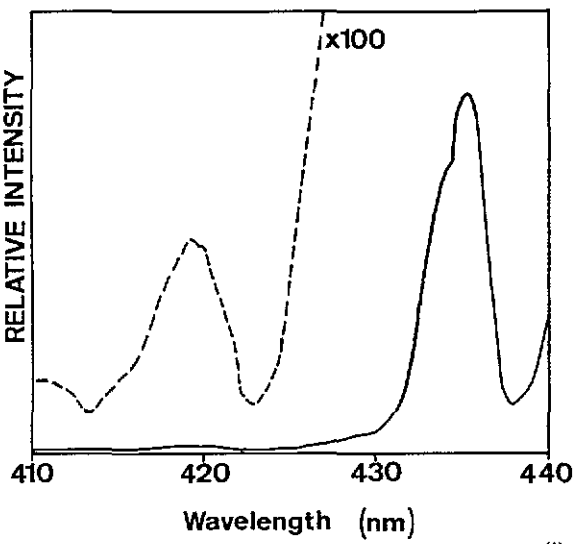

Figure 6. One- and two-phonon vibronic replicas in the $^3H_4^{(1)} \rightarrow {}^3P_2$ excitation spectrum of the $^3P_0 \rightarrow {}^3F_2$ emission of Pr^{3+} in $Na_5La(MoO_4)_4$:0.5 mol% Pr^{3+} at 4.2 K. The zero-phonon origin is at 450.6 nm, the one-phonon replica is at 435.0 nm (~ 800 cm^{-1} from the zero-phonon origin) and the two-phonon replica is at 419.5 nm (~ 1600 cm^{-1} from the zero-phonon origin).

Two-phonon vibronic replicas are only expected for Δ process vibronics [1, 28]. For a Δ process vibronic involving i phonons the ratio of the integrated vibronic intensity to the integrated zero-phonon intensity is given by [28]

$$\frac{I_{vib,i}}{I_{zp}} = \frac{e^{-S}S^i}{i!} \tag{5}$$

where S is the Huang–Rhys coupling factor.

From equation (5) and the ratio between the integrated intensities of the one-phonon replica and the zero-phonon line in the $^3H_4^{(1)} \rightarrow {}^3P_2$ excitation spectrum of the $^3P_0$ emission of Pr^{3+} in $Na_5La(MoO_4)_4$:0.05 mol% Pr^{3+}, we estimate S to be 0.02. The ratio $I_{vib,2}/I_{vib,1}$ is therefore expected to be 0.01 (i.e. $S/2$), which is in good agreement with the experimental value of 0.01, estimated for a sample with 0.5 mol% Pr^{3+}.

Two-phonon vibronic replicas are also observed for the isostructural tungstate lattice. The coupling factor S is estimated to be 0.01. The expected $I_{vib,2}/I_{vib,1}$ ratio is thus 0.005, which is in good agreement with the experimental value, 0.004. The Huang–Rhys coupling factor S of Pr^{3+} appears to be larger in $Na_5La(MoO_4)_4$ than in $Na_5La(WO_4)_4$, consistent with the larger degree of covalency experienced by the Pr^{3+} ions in the former host lattice. As mentioned above (section 3.1), the higher degree of covalency of the Pr–O bonds in the molybdate lattice is reflected by the shift of the emission and excitation spectra of Pr^{3+} to lower energies, in comparison to those in the isostructural tungstate. The good agreement

between the expected and the experimental $I_{vib,2}/I_{vib,1}$ values strongly suggests that the vibronic coupling of Pr^{3+} in these host lattices is to a great extent due to the Δ process.

4. Conclusions

One- and two-phonon vibronic replicas are observed in the $^3H_4^{(1)} \rightarrow {}^3P_2$ excitation spectra of the $^3P_0 \rightarrow {}^3F_2$ emission of Pr^{3+} in $Na_5La(MO_4)_4$ (M=Mo, W) at 4.2 K. The good agreement between the expected and the observed relative intensities of the two-phonon replicas strongly suggests that the vibronic coupling strength of Pr^{3+} in these host lattices is dominated by the Δ process contribution. This conclusion is corroborated by the observed host lattice dependence of the transition probability A_{vib} for the vibronic transitions in the $^3H_4^{(1)} \rightarrow {}^3P_0$ excitation spectra, and by the breakdown of the $U^{(2)} \neq 0$ selection rule for the $^3H_4^{(1)} \rightarrow {}^3P_{0,2}$ excitation and the $^3P_0 \rightarrow {}^3F_2$ emission transitions of Pr^{3+}.

Acknowledgments

The authors are indebted to Professor J H van der Maas and Mr E Th G Lutz (Utrecht University) for measuring the vibrational spectra of $Na_5La(MO_4)_4$. CMD gratefully acknowledges the award of a scholarship by CNPq (Brazilian Agency). S Schenker wishes to thank the ERASMUS exchange program for financial support.

References

[1] Miyakawa T 1973 *Luminescence of Crystals, Molecules and Solutions* ed F Williams (New York: Plenum) p 394
[2] Henderson B and Imbusch G F *Optical Spectroscopy of Inorganic Solids* (Oxford: Oxford University Press) ch 5
[3] Blasse G 1992 *Int. Rev. Phys. Chem.* **11** 71
[4] Judd B R 1980 *Phys. Scr.* **21** 543
[5] Faulkner T R and Richardson F S 1978 *Mol. Phys.* **35** 1141
[6] Dexpert-Ghys J and Auzel F 1984 *J. Chem. Phys.* **80** 4003
[7] de Mello Donegá C, Meijerink A and Blasse G 1992 *J. Phys.: Condens. Matter* **4** 8889
[8] de Mello Donegá C and Meijerink A 1993 *J. Lumin.* **55** 315
[9] Meijerink A, de Mello Donegá C, Ellens A, Sytsma J and Blasse G 1994 *(Proc. DPC'93) J. Lumin.* **58** 26
[10] de Mello Donegá C, Lambaerts H, Meijerink A and Blasse G 1993 *J. Phys. Chem. Solids* **54** 873
[11] Baran E J, Vassalo M B, Cascales C and Porcher P 1993 *J. Phys. Chem. Solids* **54** 1005
[12] van Vliet J P M and Blasse G 1990 *J. Solid State Chem.* **85** 56
[13] de Mello Donegá C, Meijerink A and Blasse G *J. Lumin.* at press
[14] Kiliaan H S, Meijerink A and Blasse G 1986 *J. Lumin.* **35** 155
[15] Klevtsova R F, Glinskaya L A, Kozoeva L P and Klevtsov P V 1973 *Sov. Phys. Crystallogr.* **17** 672
[16] Efremov V A, Berezina T A, Averina I M and Trunov V K 1980 *Sov. Phys. Crystallogr.* **25** 146
[17] Tsunekawa S and Takei H 1978 *Phys. Status Solidi* A **50** 695
[18] Thoma R E, Weaver C F, Friedman H A, Insley H, Harris L A and Yakel H A 1961 *J. Phys. Chem.* **65** 1096
[19] Blasse G 1980 *Struct. Bonding* **42** 22
[20] McLanghlin R D and Conway J G 1963 *J. Chem. Phys.* **38** 1037
[21] Wong E Y, Stafsudd O M and Johnston D R 1963 *J. Chem. Phys.* **39** 786
[22] Garcia D and Faucher M 1989 *J. Chem. Phys.* **90** 5280
[23] de Mello Donegá C, Meijerink A and Blasse G unpublished
[24] Stavola M, Isganitis L and Sceats M G 1981 *J. Chem. Phys.* **74** 4228
[25] Henderson B and Imbusch G F 1989 *Optical Spectroscopy of Inorganic Solids* (Oxford: Oxford University Press) ch 10
[26] Riseberg L A and Weber M J 1976 *Relaxation Phenomena in Rare-Earth Luminescence (Progress in Optics XIV)* ed E Wolf (Amsterdam: North-Holland) p 89

[27] Moos H W 1970 *J. Lumin.* **1, 2** 106
[28] Henderson B and Imbusch G F *Optical Spectroscopy of Inorganic Solids* (Oxford: Oxford University Press) p 200
[29] Meijerink A 1993 *J. Lumin.* **55** 125
[30] Weber M J 1968 *J. Chem. Phys.* **48** 4774
[31] Downer M C 1989 *Laser Spectroscopy of Solids II* ed W M Yen (Heidelberg: Springer) ch 2
[32] Downer M C, Burdick G W and Sardar D K 1988 *J. Chem. Phys.* **89** 1787
[33] Carnall W T, Crosswhite H and Crosswhite H M 1977 Energy Level Structure and Transition Probabilities of the Trivalent Lanthanides in LaF_3 *Argonne National Laboratory Report*